The Astrophysical Journal, 688:583–596, 2008 November 20

DEEP L'- AND M-BAND IMAGING FOR PLANETS AROUND VEGA AND ϵ ERIDANI[1]

A. N. Heinze
Swarthmore College, 500 College Avenue, Swarthmore, PA 19081; aheinze1@swarthmore.edu

and

Philip M. Hinz, Matthew Kenworthy, Douglas Miller, and Suresh Sivanandam
Steward Observatory, University of Arizona, 933 North Cherry Avenue, Tucson, AZ 85721-0065;
phinz@as.arizona.edu, mkenworthy@as.arizona.edu, dlmiller@as.arizona.edu, suresh@as.arizona.edu
Received 2008 February 19; accepted 2008 July 24

ABSTRACT

We have obtained deep adaptive optics (AO) images of Vega and ϵ Eri to search for planetary mass companions. We observed at the MMT in the L' (3.8 μm) and M (4.8 μm) bands using Clio, a recently commissioned imager optimized for these wavelengths. Observing at these long wavelengths represents a departure from the H band (1.65 μm) more commonly used for AO imaging searches for extrasolar planets. The long wavelengths offer better predicted planet/star flux ratios and cleaner (higher Strehl) AO images at the cost of lower diffraction-limited resolution and higher sky background. We have not detected any planets or planet candidates around Vega or ϵ Eri. We report the sensitivities obtained around both stars, which correspond to upper limits on any planetary companions which may exist. The sensitivities of our L'- and M-band observations are comparable to those of the best H-regime observations of these stars. For ϵ Eri, our M-band observations deliver considerably better sensitivity to close-in planets than any previously published results, and we show that the M band is by far the best wavelength choice for attempts at ground-based AO imaging of the known planet ϵ Eri b. The Clio camera itself, with MMTAO, may be capable of detecting ϵ Eri b at its 2010 apastron, given a multinight observing campaign. Clio appears to be the only currently existing AO imager that has a realistic possibility of detecting ϵ Eri b.

Subject headings: instrumentation: adaptive optics — planetary systems — stars: individual (Vega, ϵ Eridani) — techniques: image processing

1. INTRODUCTION

Early space-based observations with *IRAS* identified four bright, nearby stars with strong IR excesses: β Pic, Vega, Fomalhaut, and ϵ Eri (Aumann et al. 1984; Aumann 1985). The only reasonable explanation for these excesses is that the systems contain substantial dust, which is warmed by starlight until it radiates brightly in the IR because of the large total surface area of its numerous small grains (see, e.g., Backman 1996; Li & Lunine 2003; Deller & Maddison 2005).

The dust in these systems cannot be primordial but must be continually generated by the grinding down of larger bodies such as asteroids (Backman 1996; Li & Lunine 2003; Deller & Maddison 2005). The stars are therefore said to have "debris disks." The clear implication is that each of these stars has at least an asteroid belt, and probably a more extensive planetary system, because it is unlikely that an asteroid belt would form without planets also forming, or that it would continue to grind down without ongoing gravitational stirring due to planets.

Theoretical models (e.g., Burrows et al. 2003; Baraffe et al. 2003) predict that it should be possible to make direct images of giant planets orbiting nearby young stars using the current generation of large ground-based telescopes with adaptive optics (AO). These observations are only possible at near-IR wavelengths from about 1 to 5 μm, where giant planets are self-luminous due to the gravitational energy converted to internal heat in their formation and subsequent slow contraction. Because giant planets radiate this energy away over time, they become cooler and fainter as they age. The youngest nearby stars are therefore the most promising targets for AO surveys attempting to image self-luminous giant planets.

Each of the four debris-disk stars discovered using *IRAS* is relatively young, so orbiting giant planets might be detectable if any exist. We have imaged the two stars most easily observable from Northern Hemisphere sites: Vega and ϵ Eri. Vega's age is about 0.3 Gyr (Song et al. 2001), while the age of ϵ Eri is about 0.56 Gyr (Fischer 1998). Besides the dust-dispersion timescale argument mentioned above for the existence of planetary systems around these stars, asymmetries in the dust distributions around each have led to hypotheses that the dust is being gravitationally sculpted by giant planets orbiting at large distances (Ozernoy et al. 2000; Quillen & Thorndike 2002; Wyatt 2003; Wilner 2004; Deller & Maddison 2005; Marsh et al. 2006). In the case of Vega there are suggestions that the dust may reveal the mass and approximate position of a giant planet (Wilner 2004; Deller & Maddison 2005). For ϵ Eri, in addition to evidence for a planet in a distant orbit that may be sculpting the dust (Deller & Maddison 2005; Benedict et al. 2006), there is the radial velocity (RV) and astrometric detection of the closer-in planet ϵ Eri b (Benedict et al. 2006). The combination of RV and astrometry observations permits a full orbital solution yielding ephemerides for the separation and position angle of ϵ Eri b (Benedict et al. 2006), making this the most promising case yet where attempts to image a known extrasolar planet can target a specific location.

Most imaging searches for extrasolar planets to date have used either the H band (1.5–1.8 μm) or other filters in the same wavelength regime (see, e.g., Neuhäuser et al. 2000; Masciadri et al. 2005; Biller et al. 2006, 2007; Geissler et al. 2007; Lafrenière et al. 2007). The magnitude versus mass tables of Baraffe et al. (2003) and the theoretical spectra of Burrows et al. (2003) show clearly why the H band is usually chosen: giant planets are predicted to

[1] Observations reported here were obtained at the MMT Observatory, a joint facility of the University of Arizona and the Smithsonian Institution.

be very bright at these wavelengths, much brighter than blackbodies at their effective temperatures. Detector formats are large, technology well developed, and sky backgrounds faint at the H band relative to longer wavelengths.

However, theoretical models indicate that planet/star flux ratios are much more favorable at the longer wavelength L' and M bands (3.4–4.1 and 4.5–5.0 μm, respectively). For planets at sufficiently large separations or orbiting faint stars, the planet/star flux ratio is not relevant. Rather, it is the planet's brightness relative to the sky background and/or detector read noise that matters. In this regime the very high sky background in the L' and M bands prevents them from being as sensitive as the H-band regime. However, close to very bright stars the background becomes irrelevant, and only the planet/star flux ratio matters. Under these circumstances, using the longer wavelengths makes sense.

Vega is a magnitude 0.0 standard star and is among the brightest stars in the sky at almost any wavelength. While not impressive at visible wavelengths, ϵ Eri is a very bright magnitude 1.9 at the H band. The stars are therefore excellent targets for Clio, an L'- and M-band optimized AO camera that had its first light on the MMT in 2005 June (Hinz et al. 2006). We have made deep $\sim$1 hr integrations in both the L' and M bands on both stars. Our M-band observations are the deepest ground-based images yet published in this band.

In § 2 we present our observations and data analysis strategy. In § 3 we describe our methods of analyzing our sensitivity and present our sensitivity results. Blind sensitivity tests in which simulated planet images were inserted directly into the raw data show that we have obtained 100% completeness for sources at 10 σ significance, 77% completeness for 7 σ sources, and 41% completeness for 5 σ sources, where σ is an estimate of the rms noise amplitude in the image at the spatial scale of the PSF core (the relevant scale for detection of faint point sources). We note that no other planet-imaging papers to date present such careful blind tests in their sensitivity analyses, and the fact that our tests result in somewhat lower completeness values at each significance level than might have been expected suggests such tests should always be attempted and may result in a need to revise some sensitivity estimates to more conservative values.

In § 4 we compare the sensitivity we have obtained around Vega to that of other deep observations of Vega and to the expected brightness of planets that have been hypothesized to explain the dust distribution. In § 5 we present the same comparisons for ϵ Eri, and in § 6 we present the conclusions of our study.

2. OBSERVATIONS AND DATA ANALYSIS

2.1. *The Instrument*

The Clio instrument we used for our observations has been well described elsewhere (Freed et al. 2004; Sivanandam et al. 2006; Hinz et al. 2006). We present only a brief overview here.

The MMT AO system delivers a lower thermal background than other AO systems because it uses the world's first deformable secondary mirror, thereby avoiding the multiple warm-mirror reflections (each adding to the thermal background) that are needed in AO systems where the deformable mirror is not the secondary. This unique property makes the MMT ideal for AO observations in wavelengths such as the L' and M bands that are strongly affected by thermal glow. Clio was developed to take advantage of this to search for planets in these bands. It saw first light as a simple imager offering f/20 and f/35 modes. The design allowed for coronagraphic capability, which has since been developed (Kenworthy et al. 2007) but was not fully operational at the time of our Vega and ϵ Eri observations. In the f/20 mode we used for all the observations of Vega and ϵ Eri, Clio's field of view is $15.5'' \times 12.4''$. Its plate scale is $0.04857'' \pm 0.00003''$ pixel^{-1}, which gives finer than Nyquist sampling of the diffraction-limited PSF of the MMT in the L' and M bands.

2.2. *Observing Strategy*

We carry out L'- and M-band imaging with Clio using the technique of nod subtraction, in which we take images of our target star in two different telescope positions typically offset by about $5.5''$ and then subtract the images taken in one position from those taken in the other to remove artifacts from the bright sky background and detector imperfections. Since the star is present on images taken in both positions, both provide useful science data. Nod subtraction does result in a dark negative image of the star, reducing the sensitivity in part of each image, but the area affected is fractionally small and far ($5.5''$) from the star, where planets are less likely to be found, and can be placed away from objects of potential interest by a good choice of nod direction. We also have alternative ways of processing nodded data that do away with the dark images entirely.

We typically nod the telescope every 2–5 minutes, which appears to be fast enough that variations in the sky background are sampled well enough to be essentially removed. We take 5 or 10 images in each nod position, each of which typically represents about 20 s worth of data. A full data set consists of 100–500 such images.

We choose the exposure for most of the images so that the sky background level is about 70% of the detector full well capacity. At such exposure times the cores of bright stars such as Vega and ϵ Eri are saturated, but optimal sensitivity is obtained to faint point sources beyond the saturation radii. When possible, we interleave a few nod cycles of shorter exposures yielding unsaturated star images into the sequence of longer exposure images. This allows us to measure the unsaturated PSF under the exact conditions of a particular observing sequence. We achieved the PSF measurement with ϵ Eri, but Vega proved too bright for us to reasonably obtain unsaturated images. We used other stars observed close in time to our Vega observations to provide a reference PSF for the Vega data.

Tables 1 and 2 give details of our observations. The 2006 June M-band Vega observations had far higher sky noise than the 2006 April data, possibly because of the higher thermal background during warm summer weather, and therefore were not used in calculating the final sensitivity.

2.3. *Data Analysis*

Our Clio image-processing pipeline will be described in more detail in a future paper. Here we briefly state that our baseline processing involves dark subtraction; flat-fielding; nod subtraction; several iterations of different types of deviant ("hot") pixel removal; a pattern noise correction (Fig. 1*b* shows an example image at this stage); shifting, rotation, and zero-padding in a single bicubic spline operation; final stacking; and unsharp masking of the stacked image using a Gaussian kernel 3–4 times wider than the PSF.

For the final image stacks we use a creeping mean algorithm with 20% rejection. This algorithm works by finding the mean of all values for a given pixel, rejecting the most deviant one, finding the new mean, rejecting the new maximally deviant value, etc., until the specified rejection fraction is reached. For data sets where ghosts or other artifacts can render a large fraction of the data at a given location deviant, the creeping mean produces a cleaner final stack than the median. Figure 1*a* shows an example of a raw image, Figure 1*b* shows a partially processed version of

TABLE 1
OBSERVATIONS OF SCIENCE TARGETS: BASIC PARAMETERS

Star	Date of Obs.	Band	Clio Int. (ms)	Co-adds	No. of Images
Vega	2006 Apr 12	L'	2000	10	160
Vega	2006 Apr 13	M	200	90	110
Vega	2006 Jun 10	M	100	50	558
Vega	2006 Jun 11	M	120	100	180
ϵ Eri	2006 Sep 9	M	130	100	180
ϵ Eri	2006 Sep 11	L'	1500	15	184

NOTES.—"Clio int." refers to the nominal single-frame exposure time in Clio. The integrate-while-reading mode used in high-efficiency science imaging causes the true single-frame exposure time to be about 59.6 ms longer than the nominal exposures listed here. "Co-adds" is the number of frames internally co-added by Clio to produce a single two-dimensional FITS image.

the same image just before shifting and rotation, and Figures 1*c* and 1*d* show examples of final stacked images after unsharp masking.

In addition to the image made using our baseline processing, we make images using two types of more advanced processing, one that avoids the negative star images from standard nod subtraction at the cost of slightly increased noise and one that includes subtraction of the stellar PSF using a technique similar to the angular differential imaging described by Marois et al. (2006). We use all three images when we search for companions, since the detection of a faint companion on images processed in more than one way increases the likelihood that it is real. We also construct a separate sensitivity map for each of the three differently processed master images and combine them into a single master sensitivity map. Since the different processing methods obtain optimal sensitivity at different locations, we set the sensitivity at a given location on the master map to the best sensitivity obtained at that location on any of the three separate maps. Details on how the separate sensitivity maps themselves are made may be found in § 3.

Intensive image processing such as we describe here is often used for AO planet search data, where high contrast is required and artifacts must be aggressively removed. Such processing can remove flux from the faint point sources whose detection it is intended to facilitate. Careful tests of our processing methods, however, indicate that the flux loss from a faint PSF is no more than about 10% and appears to be close to zero in most cases.

3. SENSITIVITY MEASUREMENTS AND SOURCE DETECTION TESTS

3.1. *Sensitivity Estimation*

We create a sensitivity map from each stacked master image produced by the processing outlined above. We are careful to measure the noise at the relevant spatial scale, that is, the scale of the PSF. Our method requires an unsaturated star image taken under conditions similar to those of the science data, therefore representing a good estimate of the PSF. We perform a two-parameter least-squares fit centered on each pixel in the master science image in turn, with the two parameters being the amplitude of a PSF centered on that pixel and a constant background value. This fit is performed within a disk of 6 pixels radius about each given pixel. The best-fit PSF amplitude from the fit centered on each pixel of the master science image becomes the value of the corresponding pixel of a new image: the PSF amplitude map. This PSF amplitude map image is essentially the result of PSF-fitting photometry centered in turn on every pixel in the original master science image. This PSF fitting has, of course, mostly measured simply noise; the point is that it has measured the noise at the spatial scale of the PSF.

Our method may be expected to produce results somewhat similar to the "matched filter" technique (see, e.g., Vikhlinin et al. 1995), although the least-squares fit that we use is mathematically more sophisticated than the straightforward convolution used in a matched filter. The most obvious advantage of our method is that it automatically fits and removes any slowly varying background (since our least-squares fit determines a separate background value within the disk centered on each pixel), while an ordinary matched filter requires the separate construction of a background model.

The noise in the amplitude map constructed by our PSF fitting accurately reflects the PSF-scale noise in the original image, that is, the noise at the spatial frequencies relevant for the detection of real point sources. We calculate the sensitivity at every point in the original image by computing the rms in an 8 pixel radius aperture about that point on the PSF amplitude map (for regions

TABLE 2
OBSERVATIONS OF SCIENCE TARGETS: DATA ACQUIRED

Star	Date	Band	Exposure (s)	Mean Air Mass	Rotation (deg)
Vega	2006 Apr 12	L'	3295.4	1.018	80.63
Vega	2006 Apr 13	M	2570.0	1.026	36.39
Vega	2006 Jun 10	M	4452.8	1.034	72.36
Vega	2006 Jun 11	M	3232.8	1.054	25.53
ϵ Eri	2006 Sep 9	M	3412.8	1.334	23.41
ϵ Eri	2006 Sep 11	L'	4304.5	1.342	36.92

NOTES.—The observations in June were plagued with high sky noise, which may have been due to the higher thermal background during warm summer weather. Adding them to the April *M*-band data on Vega did not significantly increase the sensitivity to objects far from the star, although in the speckle-dominated regime near the star, the sensitivity did increase by about 40%.

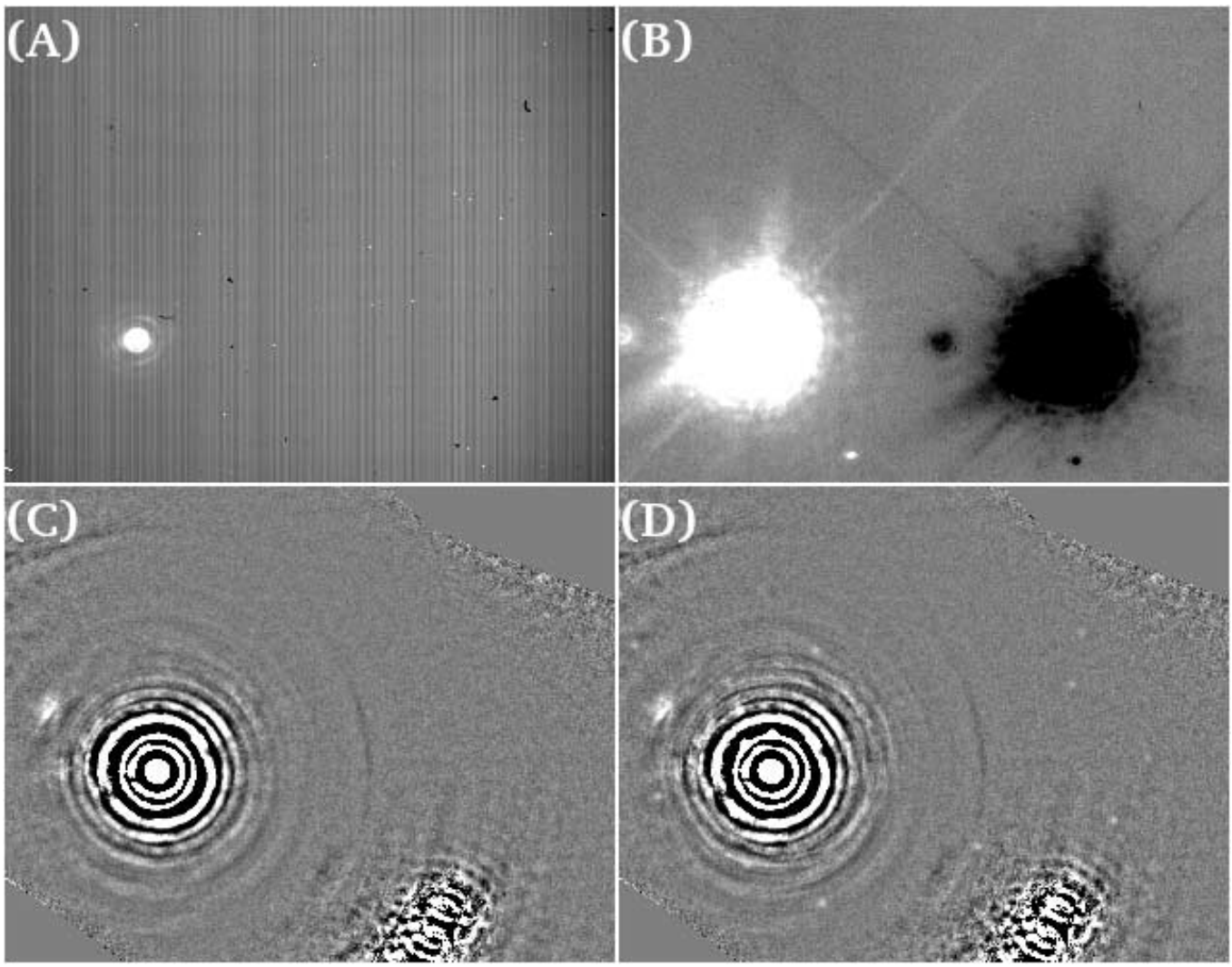

FIG. 1.—(*a*) Raw, single *M*-band image of Vega. (*b*) Nod-subtracted, processed version of the same image just before shift and rotation. The contrast is stretched 100 times more than in (*a*). (*c*) Final master *M*-band image of Vega, consisting of 110 (*b*)-like images, shifted, rotated, and co-added. The contrast is stretched 10 times more than in (*b*). (*d*) Like (*c*), but with fake planets added to the raw data. The field shown in all panels is about $15.5'' \times 12.5''$. The unsharp masking which has removed the bright stellar halo in (*c*) and (*d*) is responsible for the black spaces between the inner diffraction rings. The noisy region at the bottom right in these panels is due to the negative stellar images from nod subtraction.

too close to the star, where a circular aperture would not produce accurate results, we use a 45 pixel long arc at constant radius from the star instead). Note that since the data are only slightly oversampled, both the 8 pixel radius disk and the 45 pixel long arc span many resolution elements or speckles. Calculating the rms on the PSF amplitude map rather than the original master image takes into account spatial correlations between pixels (i.e., the fact that the noise in adjacent pixels is not independent). This is a large effect in the case of speckle noise.

We note that many previous planet-imaging papers have not used a sensitivity estimator mathematically able to account for correlated noise in speckles, or at least have not devoted sufficient space to the description of their sensitivity estimator to make it clear whether it properly measures correlated noise. Estimators that contain an implicit mathematical assumption that the noise is independent from one pixel to the next can significantly overestimate the sensitivity in speckle-dominated regions close to the star. The careful design, description, and testing of sensitivity estimators is an important task, because in the case of a nondetection all the science rests on upper limits set through sensitivity estimation. The only observational planet-imaging paper we are aware of prior to this work in which a sensitivity estimator able to account for correlated noise is clearly described is Lafrenière et al. (2007). (However, we may safely assume that Marois et al. [2006] used the same estimator as Lafrenière et al. [2007]. Hinkley et al. [2007] also used, and carefully described, such an estimator in their paper to set limits on brown dwarfs in close orbits around Vega.)

3.2. *Testing the Sensitivity Estimator*

To test the accuracy of our sensitivity estimator, we conducted blind tests in which fake planets were inserted into the raw data. The altered images were then processed in exactly the same way as the original raw data, and the "planets" were detected using both automatic and manual methods by an experimenter who knew neither their positions nor their numbers. These planets were inserted at fixed nominal significance levels of 10 σ, 7 σ, and 5 σ based on the sensitivity map. We conducted such tests for each of our four data sets (the L'- and *M*-band data sets for each of the two stars). The final result of each test was that every inserted planet was classified as "Confirmed," "Noticed," or "Unnoticed." "Confirmed" means the source was confidently detected and

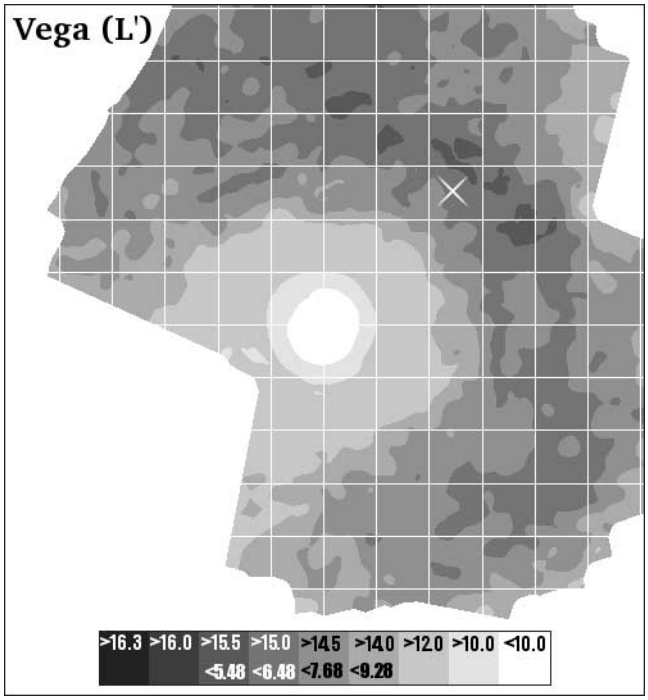

FIG. 2.—The 10 σ sensitivity contour map for our Vega L' observations in magnitudes. The grid squares superposed on the figure for astrometric reference are $2'' \times 2''$. The approximate location of the hypothetical planet from Wilner (2004) is marked with a white cross. The best areas in this image give sensitivity to objects fainter than $L' = 15.5$. The numbers at the top of the color bar give the sensitivity of each contour in magnitudes, while the numbers at the bottom give the equivalent value in M_J, where applicable, based on the models of Burrows et al. (2003) with the age set to 0.3 Gyr.

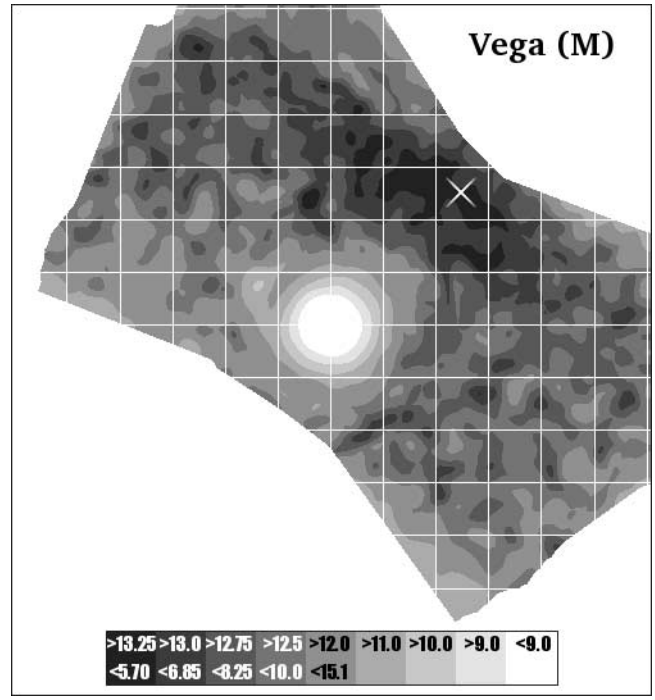

FIG. 3.—The 10 σ sensitivity contour map for our Vega M observations in magnitudes. The grid squares superposed on the figure for astrometric reference are $2'' \times 2''$. The approximate location of the hypothetical planet from Wilner (2004) is marked with a white cross. The numbers at the top of the color bar give the sensitivity of each contour in magnitudes, while the numbers at the bottom give the equivalent value in M_J, where applicable, based on the models of Burrows et al. (2003) with the age set to 0.3 Gyr.

certainly worthy of long-exposure follow-up observations at the MMT. If a source is detected with this confidence level in an unaltered data set, there is no significant doubt that it is a real object. In calculating our completeness, we count only confirmed sources as true detections. "Noticed" means the source was flagged by our automatic detection algorithm or noticed as a possible real object during the purely manual phase of planet searching but it cannot be confirmed beyond reasonable doubt. Many spurious sources are "Noticed," whereas the false-positive rate for "Confirmed" detections is extremely low, with none for any of the data sets discussed here. "Unnoticed" means a fake planet was not automatically flagged or noticed manually.

The end result of the four blind sensitivity tests was that at 10 σ, 50 of 50 total inserted planets were confirmed, giving us 100% completeness to the limits of the statistical accuracy of the test. At 7 σ, 23 of 30 total inserted sources were confirmed, giving us 77% completeness, and 29 of the 30 sources were at least noticed. At 5 σ, 11 of 27 total inserted planets were confirmed, for 41% completeness, and 23 of the 27 sources were at least noticed. In addition to the completeness levels for confirmed sources, the percentages of fake planets that were at least noticed is of potential interest for setting limits: 100% of 10 σ sources, 97% of 7 σ sources, and 85% of 5 σ sources were at least noticed. We note that if we had quoted 5 σ sensitivities without conducting a blind sensitivity test we would have significantly overestimated our true high-completeness sensitivity. Most papers in the field of planet-imaging surveys do in fact quote 5 σ limits and do not verify their validity by a blind test.

In our sensitivity experiments there were no false positives among the "Confirmed" sources. Many spurious sources were classified as "Noticed," which is why we do not count "Noticed" sources as detections for completeness purposes. The conclusion of our fake-planet experiments is that our detection strategy has an extremely low false-alarm probability and delivers the completeness values given above. The fact that a large majority of low-significance sources were noticed, even if not confirmed, indicates that upper limits stronger than those implied by our formal completeness values may be set on planets in clean regions of an image where no spurious sources were noticed.

3.3. *Final Sensitivity Results*

We have converted the master sensitivity maps described above into magnitude contour images, with 10 σ sensitivity values shown. We quote sensitivities in apparent magnitudes based on observations of photometric standard stars (from Leggett et al. 2003), rather than giving Δ-magnitudes relative to the primary. We present our L'- and M-band Vega results in Figures 2 and 3, with the approximate position of the hypothetical planet from Wilner (2004) marked with a white cross. Figures 4 and 5 present the analogous results for ϵ Eri. Our Vega M-band observation is the deepest ground-based M-band observation yet published.

We have further translated our master sensitivity map for each data set into 10 σ sensitivity curves and plotted them in Figures 6–13. Our sensitivity varies azimuthally, as well as radially, due to the negative nod-subtraction images, ghosts, and different distances to the edge of the valid data region in different directions. Therefore, we have computed both the 50th and 90th percentile sensitivities at each radius. Both are shown, with the 50th percentile of course indicating our median sensitivity and the 90th percentile indicating our sensitivity in the cleanest 10% of the image at a given radius from the star. We have also indicated the "Confirmed," "Noticed," and "Unnoticed" planets from our sensitivity tests with appropriate symbols. The sensitivity in

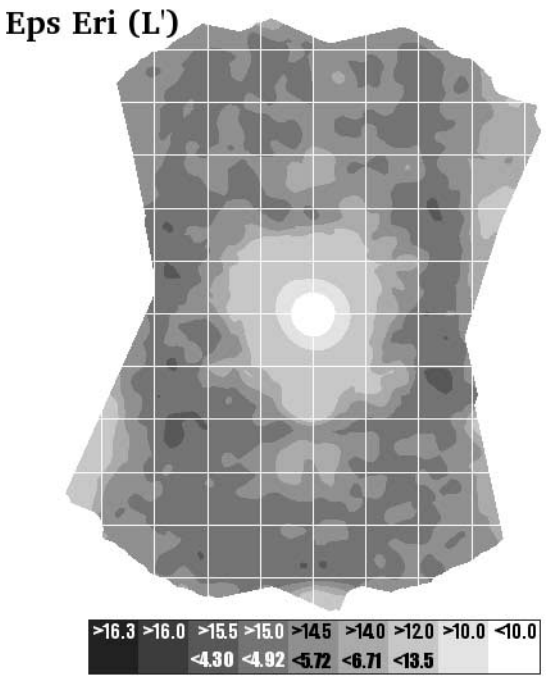

FIG. 4.—The 10 σ sensitivity contour map for our ϵ Eri L' observations in magnitudes. The best areas in this image give sensitivity to objects fainter than $L' = 15.5$. The grid squares superposed on the figure for astrometric reference are $2'' \times 2''$. The numbers at the top of the color bar give the sensitivity of each contour in magnitudes, while the numbers at the bottom give the equivalent value in M_J, where applicable, based on the models of Burrows et al. (2003) with the age set to 0.56 Gyr.

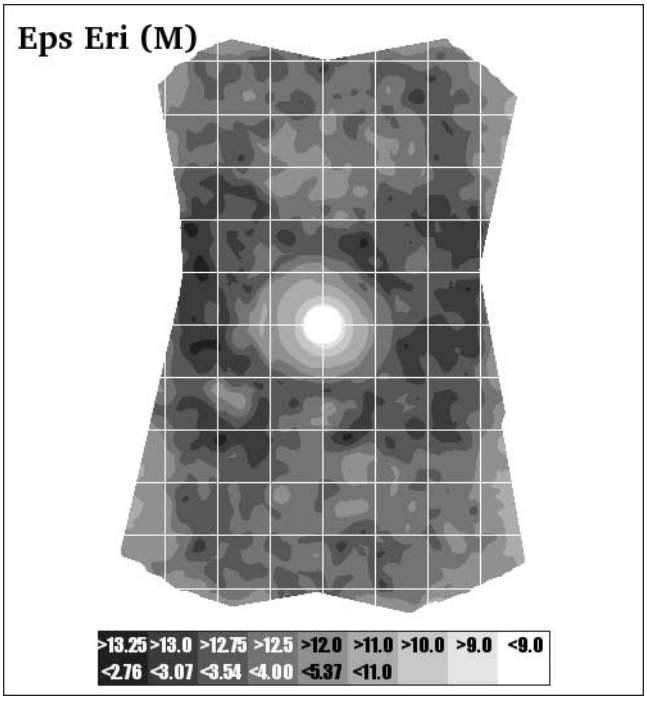

FIG. 5.—The 10 σ sensitivity contour map for our ϵ Eri M observations in magnitudes. The grid squares superposed on the figure for astrometric reference are $2'' \times 2''$. The numbers at the top of the color bar give the sensitivity of each contour in magnitudes, while the numbers at the bottom give the equivalent value in M_J, where applicable, based on the models of Burrows et al. (2003) with the age set to 0.56 Gyr.

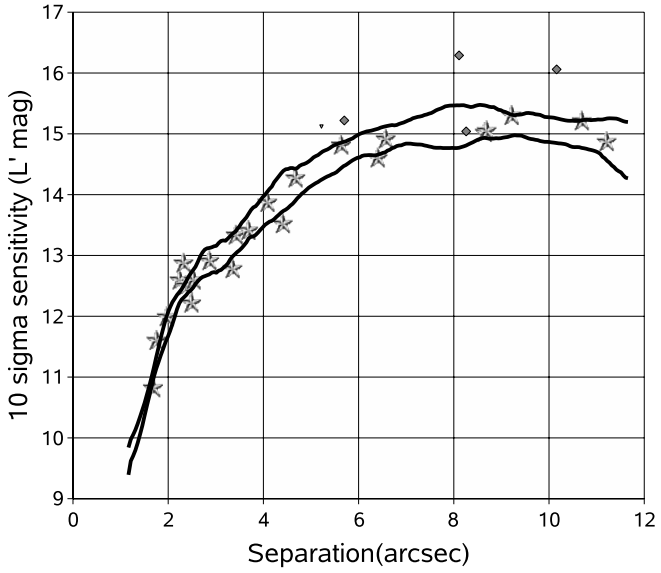

FIG. 6.—The 10 σ sensitivity of our Vega L'-band observations in magnitudes, plotted against separation in arcseconds. The 50th and 90th percentile sensitivity curves are shown, along with fake planets from the blind sensitivity test. The stars represent fake planets that were confidently detected, the diamonds represent those that were suspected but not confirmed, and the tiny triangle represents the only fake planet that was not at least suspected.

these plots increases with separation from the star, as one would expect, but then decreases again as the edge of the good data region (i.e., the useful field on the master stacked images) is reached. The noise goes up at the edge of the useful field because, due to the shifts and rotations required to register the images, the coverage (the number of images supplying data to a given pixel) goes down near the edge of the field.

Figures 6 and 7 show the sensitivity we obtained in our L' observations of Vega, first in "observational" units of sensitivity in

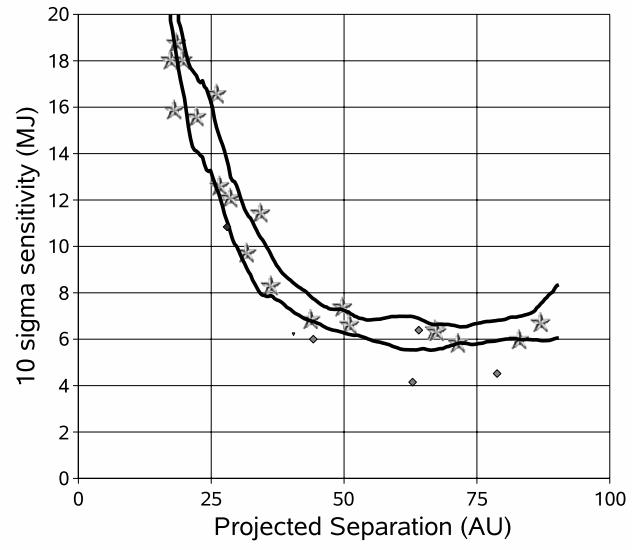

FIG. 7.—Sensitivity of our Vega L'-band observations in terms of the minimum mass for a planet detectable at the 10 σ level in M_J, plotted against projected separation in AU. The magnitude-mass conversion was done using the Burrows et al. (2003) models for an age of 0.3 Gyr. The 50th and 90th percentile sensitivity curves are shown, along with fake planets from the blind sensitivity test. The stars represent fake planets that were confidently detected, the diamonds represent those that were suspected but not confirmed, and the tiny triangle represents the only fake planet that was not at least suspected.

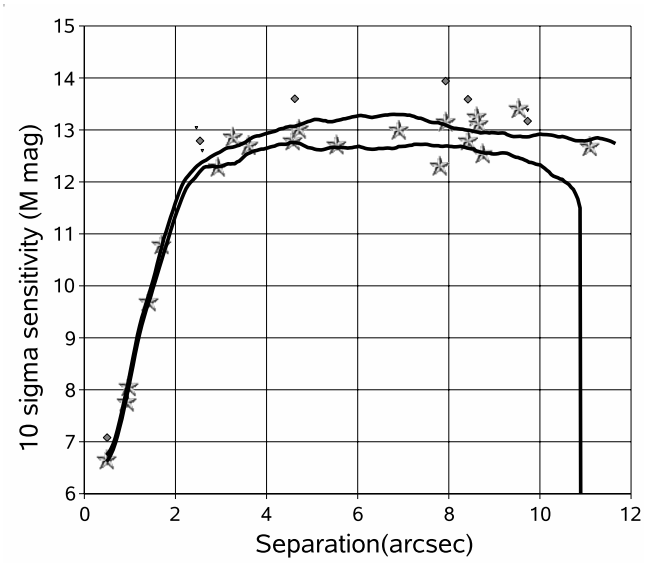

FIG. 8.—The 10 σ sensitivity of our Vega M-band observations in magnitudes, plotted against separation in arcseconds. The 50th and 90th percentile sensitivity curves are shown, along with fake planets from the blind sensitivity test. The stars represent fake planets that were confidently detected, the diamonds represent those that were suspected but not confirmed, and the tiny triangles are those that were not suspected.

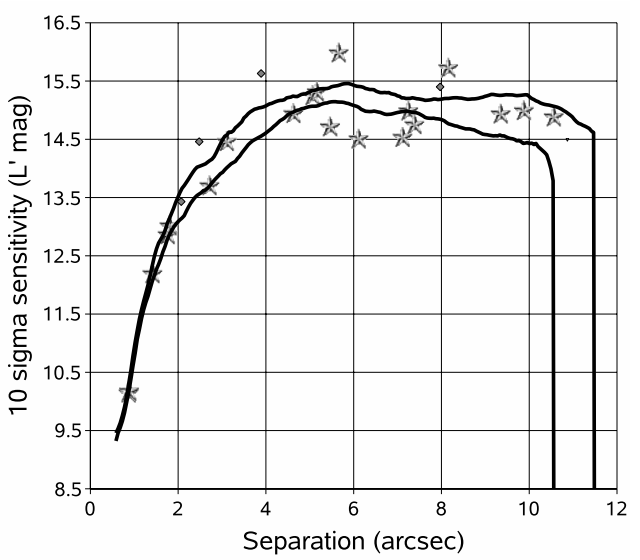

FIG. 10.—The 10 σ sensitivity of our ϵ Eri L'-band observations in magnitudes, plotted against separation in arcseconds. The 50th and 90th percentile sensitivity curves are shown, along with simulated planets from the blind sensitivity test. The stars represent fake planets that were confidently detected, the diamonds represent those that were suspected but not confirmed, and the tiny triangle represents the only fake planet that was not at least suspected.

magnitudes versus separation in arcseconds and then in "physical" units of M_J (based on the Burrows et al. [2003] models and adopting a 0.3 Gyr age for Vega [Song et al. 2001]) versus projected separation in AU. Vega has approximately magnitude 0.0 at every band, so the magnitudes in Figure 6 correspond approximately to Δ-magnitude values. Figures 8 and 9 show the sensitivity obtained in our M-band observations of Vega, following exactly the same conventions as the L' figures that precede them.

Comparison of Figures 7 and 9 shows that the L'- and M-band results provided similar sensitivity to planets around Vega. The M-band results are slightly better, especially at smaller separations. This is not surprising, because the predicted planet/star flux ratio is even more favorable at the M band than at L'. Also, MMTAO, like all AO systems, delivers better Strehl ratios at longer wavelengths, so the PSF subtraction is more effective at the M band than at L'.

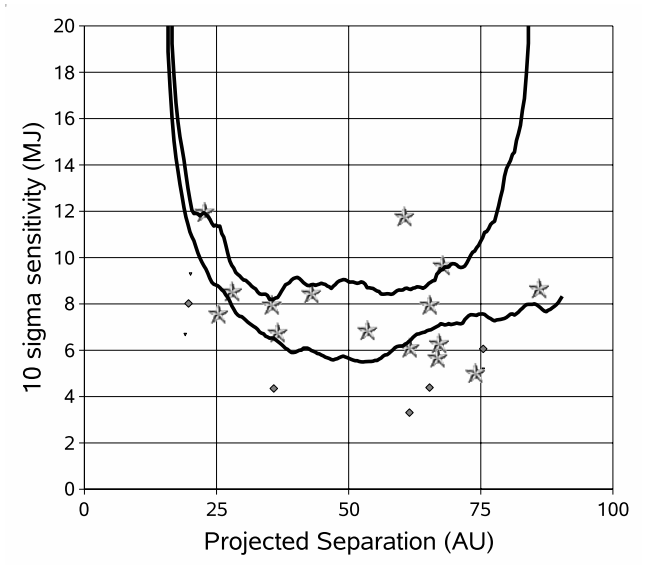

FIG. 9.—Sensitivity of our Vega M-band observations in terms of the minimum mass for a planet detectable at the 10 σ level in M_J, plotted against projected separation in AU. The magnitude-mass conversion was done using the Burrows et al. (2003) models for an age of 0.3 Gyr. The 50th and 90th percentile sensitivity curves are shown, along with fake planets from the blind sensitivity test. The stars represent fake planets that were confidently detected, the diamonds represent those that were suspected but not confirmed, and the tiny triangles are those that were not suspected.

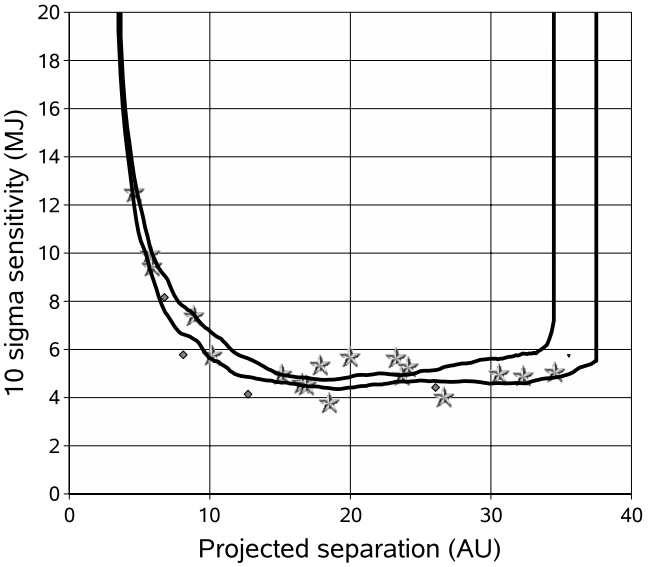

FIG. 11.—Sensitivity of our ϵ Eri L'-band observations in terms of the minimum mass for a planet detectable at the 10 σ level in M_J, plotted against projected separation in AU. The magnitude-mass conversion was done using the Burrows et al. (2003) models for an age of 0.56 Gyr. The 50th and 90th percentile sensitivity curves are shown, along with fake planets from the blind sensitivity test. The stars represent fake planets that were confidently detected, the diamonds represent those that were suspected but not confirmed, and the tiny triangle represents the only fake planet that was not at least suspected.

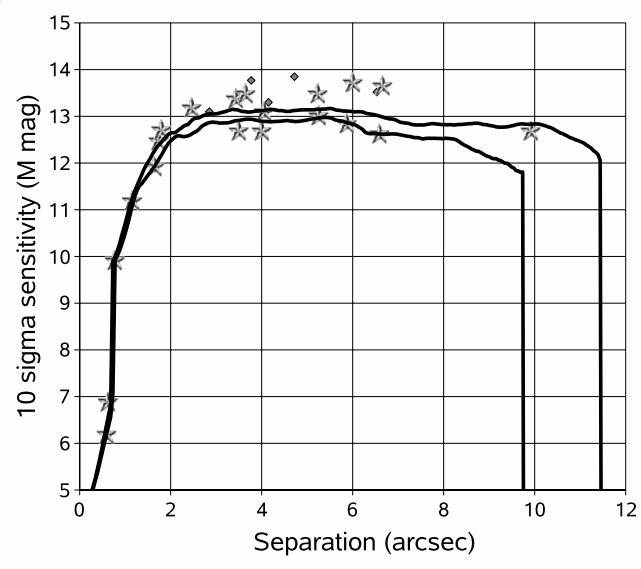

FIG. 12.—The 10 σ sensitivity of our ϵ Eri M-band observations in magnitudes, plotted against separation in arcseconds. The 50th and 90th percentile sensitivity curves are shown, along with simulated planets from the blind sensitivity test. The stars represent fake planets that were confidently detected, and the diamonds represent those that were suspected but not confirmed. In the sensitivity test for this data set, all of the fake planets were at least suspected.

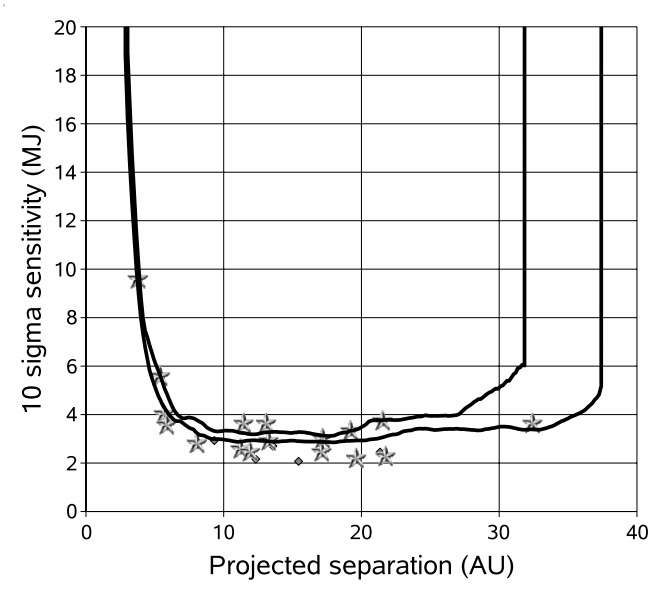

FIG. 13.—The 10 σ sensitivity of our ϵ Eri M-band observations in terms of minimum detectable planet mass in M_J, plotted against projected separation in AU. The magnitude-mass conversion was done using the Burrows et al. (2003) models for an age of 0.56 Gyr. The 50th and 90th percentile sensitivity curves are shown, along with fake planets from the blind sensitivity test. The stars represent fake planets that were confidently detected, and the diamonds represent those that were suspected but not confirmed. In the sensitivity test for this data set, all of the fake planets were at least suspected.

Figures 10–13 show the sensitivity of our L'- and M-band observations of ϵ Eri, following the same conventions as the Vega figures that precede them. For ϵ Eri we have adopted an age of 0.56 Gyr (Fischer 1998). Note that the magnitudes in Figures 10 and 12 may be converted to Δ-magnitudes by subtracting the L' magnitude of ϵ Eri, which is about 1.72 (the $L' - M$ color of the star is near zero).

Comparing Figure 11 with Figure 13 shows that for ϵ Eri, the advantage of the M band over L' is considerably more than for Vega. The fundamental reason for this is that ϵ Eri is closer to us than Vega. This is an important point we will refer back to later; the smaller the distance to a star system, the more favorably long-wavelength planet-search observations of the system will compare to short-wavelength ones. There are several logical links in the explanation of this observational fact. First, intrinsically low-luminosity planets can be detected only in the nearest systems. Second, low-luminosity planets have low $T_{\rm eff}$. Third, low-$T_{\rm eff}$ planets have red $L' - M$ colors. Therefore, the faintest detectable planets will be more red in nearby systems than in distant ones, and it follows that longer wavelength observations (i.e., M band) will perform best relative to shorter wavelength ones (i.e., L') on the very nearest stars. This conclusion is most obvious when one considers background-limited regions of images at large separations from the star, but it applies in the contrast-limited regime as well.

4. VEGA: COMPARISON WITH OTHER STUDIES AND UPPER LIMITS FOR HYPOTHETICAL PLANETS

4.1. *Comparing Our Sensitivity with Other Studies*

We have not attempted to compare our Vega results with an exhaustive list of all previous attempts to image planets or other faint objects around Vega. Instead, we have chosen two of the best previous results: first, the H-band imaging results of Itoh et al. (2006); and second, the narrowband, H-regime images of Marois et al. (2006). The latter presents the most sensitive images yet published for substellar companions at 3″–10″ separations from Vega.

Before comparing our sensitivities with these other observations, a brief discussion about the different sensitivity estimation techniques used by the respective observers is in order. As described above, in this work we have used an estimator able to account for correlated noise, performed blind tests of our sensitivity estimator, and quoted 10 σ limits.

Itoh et al. (2006) did not calculate sensitivity limits in terms of σ. Instead, they calculated their sensitivities by performing numerous tests in which they placed four planets into their data at a fixed separation and Δ-magnitude with respect to the primary. These tests differ from our own blind sensitivity tests in that the locations of the Itoh et al. (2006) fake planets were known and fixed from one test to the next. Itoh et al. (2006) set their sensitivity at each separation to the faintest Δ-magnitude at which at least three of the four planets were recovered by their automatic detection algorithm. Therefore, the Itoh et al. (2006) sensitivities correspond to planet brightness values at which they have at least 75% completeness with an unknown false-positive rate. Although it appears that the completeness level corresponding to the Itoh et al. (2006) sensitivities corresponds better to our 7 σ level, we have conservatively chosen to compare the Itoh et al. (2006) sensitivity values to our own 10 σ results without alteration.

Marois et al. (2006) do not explain how their quoted 5 σ sensitivity limits are obtained. We assume, however, that they used the same method as Lafrenière et al. (2007), another planet-imaging survey by a very similar set of authors, presenting observations made with the same telescope, instrument, and observing and analysis strategies. Lafrenière et al. (2007) set σ limits using a sensitivity estimator carefully designed to account for correlated noise. They also carefully account for processing losses, but they do not present blind sensitivity tests. Assuming that Marois et al. (2006) used the same good estimator and careful correction of processing losses, we conservatively choose to consider their quoted 5 σ limits

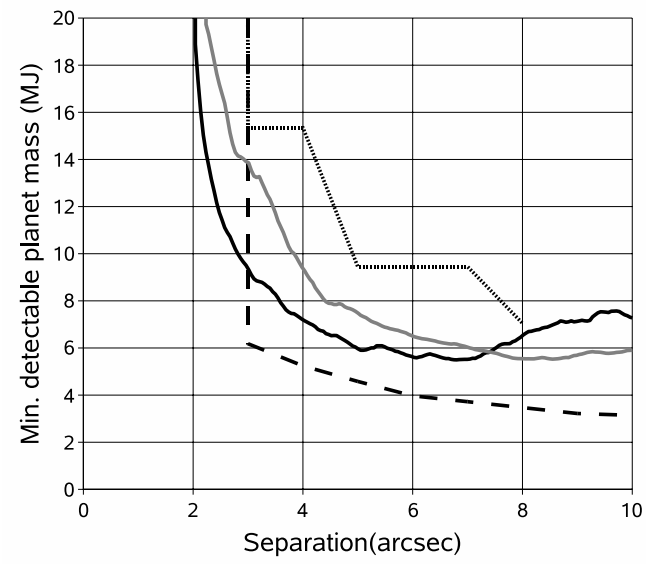

FIG. 14.— Comparison of the sensitivities obtained around Vega with different techniques. Magnitude sensitivities have been converted to planet mass limits in M_J using the theoretical models of Burrows et al. (2003) for an age of 0.3 Gyr. The dashed line indicates the narrowband *H*-regime result from Marois et al. (2006), the dotted line indicates the *H*-band result from Itoh et al. (2006), the gray solid line indicates our 90th percentile L' result, and the black solid line indicates our 90th percentile *M*-band result.

to be comparable with our 7 σ limits. Based on this assumption we transform them to 10 σ limits for comparison with our own. We also adjust their limits by a factor of 2 (0.753 mag) in the direction of greater sensitivity, in order to scale from the planet-optimized narrowband filter they used to the broadband *H* filter. (Lafrenière et al. [2007] estimate this correction at a factor between 1.5 and 2.5; we have used the mean value of 2.0.)

Figure 14 shows the sensitivities of our Vega L'- and *M*-band observations compared to those of Itoh et al. (2006) and Marois et al. (2006). The magnitude limits, adjusted as described above, have been converted to planet masses using the theoretical planet models of Burrows et al. (2003), adopting the Song et al. (2001) age of 0.3 Gyr. We plot our 90th percentile 10 σ sensitivity values, because the 90th percentile curves are smoother and easier to interpret and sensitivity at least this good can be obtained at a position angle of choice by a well-tuned observing strategy. Although our observations are more sensitive to planetary mass objects around Vega than the observations of Itoh et al. (2006), the carefully processed narrowband observations of Marois et al. (2006) are more sensitive than ours by $1.5M_J$–$3M_J$ at all separations beyond 3″, which was their approximate saturation radius. Inward of 3″ our images are sensitive mainly to brown dwarfs and the most massive planets, while the other plotted observations are saturated or very insensitive. However, in the regime of higher masses and smaller separations than covered by our figure, we note that Lyot project *H*-band observations of Vega (Hinkley et al. 2007) obtain sensitivity to massive brown dwarfs inward to about 0.7″. Their observations appear to be more sensitive to lower mass brown dwarfs than ours inside of 1.5″, while ours are more sensitive at 2″ and farther out.

It is interesting to note that Figure 14 would look very different if we plotted Δ-magnitude rather than minimum detectable planet mass. The sensitivity of the *H*-regime results of Marois et al. (2006) would surpass the sensitivity of our observations by a far greater margin in Δ-magnitude terms. At the L' and *M* bands the sky background is far brighter than in the *H* regime. Also, diffraction-limited resolution is several times lower, and the Airy pattern is correspondingly larger in angular terms. The result is that despite the cleaner, higher Strehl images offered by AO systems at longer wavelengths, the Δ-magnitude versus angular separation curves at the L' and *M* bands are typically considerably less good than those in the *H* regime. Because the planet/star flux ratios are so much better in the L' and *M* bands, however, when we convert from Δ-magnitudes to planet masses the sensitivity gap closes considerably, and in fact (as is seen below in the case of ϵ Eri) the longer wavelengths may turn out to be more sensitive.

In terms of planet mass, the Marois et al. (2006) *H*-band regime observations were more sensitive than our L'- and *M*-band results beyond 3″, but not by a huge margin. Theoretical planet models are still somewhat uncertain because of the dearth of observational constraints. The L'- and *M*-band observations of bright stars such as Vega make sense to diversify the investment of planet-imaging effort and hedge the overall results against the possibility that unexpected atmospheric chemistry, clouds, or evolutionary effects (see, e.g., Marley et al. 2007) cause planets to appear fainter in the *H* band than current models predict. It is also possible that planets could be fainter than predicted at the longer wavelengths, specifically *M* (Leggett et al. 2007). However, the suppression of *M*-band flux observed by Leggett et al. (2007) applies only to objects with $T_{\rm eff}$ from 700 to 1300 K. The situation for objects cooler than 700 K is unknown. According to the Burrows et al. (2003) models, our Vega *M*-band observations were sensitive to planets with $T_{\rm eff}$ below 400 K. Such objects may be too cold to have the enhanced concentrations of CO to which Leggett et al. (2007) attributed the *M*-band flux suppression (see Hubeny & Burrows 2007).

Because they offer better flux ratios relative to the primary star than shorter wavelengths, the L' and *M* bands we have used are optimal for detecting massive planets and low-mass brown dwarfs at small separations from Vega and other very bright stars.

4.2. *Upper Limits at the Locations of Hypothetical Planets*

Wilner (2004) presents high-resolution submillimeter observations of Vega which show two bright clumps arranged asymmetrically relative to the star. He states that it is very unlikely that the clumps could be background galaxies, and he is essentially certain that they are concentrations of dust in the Vega system. Furthermore, the dust could represent the remains of two different planetesimal collisions in the system, but the collisions would have to have happened fairly recently or the dust would have dispersed. Wilner (2004) therefore concludes that the most reasonable assumption is that the clumps are dust concentrations resulting from resonant interactions between the dust and a massive planet. He shows that the observations could be explained by a $3M_J$ planet in a large, eccentric orbit, which would currently be near apastron and located about 7.1″ northwest of the star (although the submillimeter observations were carried out a few years before our imaging, a planet near apastron in such a large orbit would not move appreciably over that interval).

We chose the target position and nod direction for our Vega observations to obtain good sensitivity at the location of this hypothetical planet. The planet's location is marked on our sensitivity contour plots (Figs. 2 and 3). We do not detect the planet, so our observations place upper limits on its mass.

At an approximate separation of 7.1″, P.A. 315° (due northwest), our L' images of Vega give a 10 σ sensitivity of $L' = 15.21$ or a 7 σ sensitivity of $L' = 15.60$. Translating these magnitudes to masses using the Burrows et al. (2003) models for an age of

0.3 Gyr, and using the results of our blind sensitivity tests, we can rule out a planet at this location with a mass above $6.02M_J$ with near 100% confidence and one more massive than $4.30M_J$ with 77% confidence. If the images were very clean at this location, showing no suspected sources, we could set stronger limits. However, there was a suspected source within about 0.4″ of this location. Careful records of the manual examination of the images make it clear that the suspected source can be identified as spurious with high confidence and should by no means be considered a candidate detection of the Wilner (2004) planet. Its appearance simply means that the images are not very clean at this location, and the stronger limits possible in regions without suspected sources do not apply.

At the same location on our *M*-band images, we obtained 10 σ, 7 σ, and 5 σ limits of $M = 13.39$, 13.78, and 14.14, respectively. Using the Burrows et al. (2003) models for an age of 0.3 Gyr, these magnitude limits correspond to planets of $5.14M_J$, $3.76M_J$, and $2.86M_J$, respectively. Records from our automatic and manual examination of the images show no suspected source within 1.5″ of this location. Since in the sensitivity tests 97% of 7 σ planets and 85% of 5 σ planets were at least suspected, we can rule out a planet above $3.76M_J$ at this location at the 97% confidence level and one above $2.86M_J$ at the 85% confidence level. The excellent sensitivity obtained at this location is due in part to the fact that our observing strategy was optimized to give good sensitivity near the position of the Wilner (2004) hypothetical planet.

We can set limits on the hypothetical planet of Wilner (2004) close to, or perhaps even below, the proposed mass of $3M_J$. It would appear from Figure 14 that Marois et al. (2006) set similar or slightly lower limits, although the exact sensitivity of their observations at the position angle of the Wilner (2004) planet cannot be explicitly analyzed because they present their sensitivity only in a radially averaged sense. Observations at the *H* and *M* bands have thus consistently set upper limits near the predicted mass of $3M_J$. A $3M_J$ planet at the 0.3 Gyr age we have adopted for Vega would have $T_{\rm eff}$ between 300 and 400 K. No objects in this temperature range have yet been observed, so model fluxes are not observationally constrained at any wavelength. Where an upper limit from a single band would be tentative because of the uncertainties of the models, the consistent results from a range of wavelengths allow us to conclude that it is probable no $3M_J$ planet exists at this location.

Wilner (2004) makes it clear that other models besides his hypothetical $3M_J$ planet might explain the observed dust distribution, and that further modeling is needed to see what range of planetary orbits and masses might be capable of producing the resonant dust concentrations seen in the submillimeter. Marsh et al. (2006), for example, explain the distribution of dust they observe around Vega at 350–450 μm wavelengths (vs. 850 μm for Wilner 2004) by a Neptune-mass planet in a 65 AU orbit. It is not entirely clear whether their model also explains the Wilner (2004) images; however, Wyatt (2003) presents a model of a migrating Neptune-mass planet that does match the 850 μm images. In contrast to Wyatt (2003) and Marsh et al. (2006), Deller & Maddison (2005) present a model that explains the 850 μm images by a $3M_J$ planet in a considerably larger orbit than that suggested by Wilner (2004). It would have the same current P.A. as the Wilner (2004) planet (northwest of the star, near P.A. 315°), but it would be 12″–13″ from Vega as opposed to 7″. Our Clio observations do not obtain good sensitivity at these larger separations, although new, differently targeted Clio images could.

No current observational technique can image Neptune-mass extrasolar planets in distant orbits. The nondetections of our survey and that of Marois et al. (2006) lend some support to models explaining the Vega dust distribution using such planets rather than the model of Wilner (2004), in which the planet has a mass a few times that of Jupiter. However, we cannot rule out a $3M_J$ planet in the more distant orbit suggested by Deller & Maddison (2005), simply because our observing strategy was not designed to give good sensitivity at such a large separation.

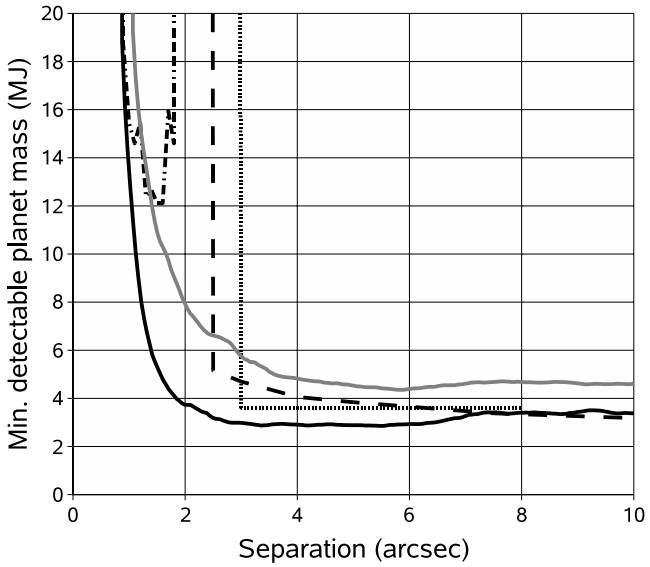

FIG. 15.—Comparison of the sensitivities obtained around ϵ Eri with different techniques. Magnitude sensitivities have been converted to planet mass limits in M_J using the theoretical models of Burrows et al. (2003) for an age of 0.56 Gyr. The dashed line indicates the narrowband *H*-regime result from Lafrenière et al. (2007), the dot-dashed line at small separations indicates the SDI result from Biller et al. (2007), the dotted line indicates the *H*-band result from Itoh et al. (2006), the gray solid line indicates our 90th percentile L' result, and the black solid line indicates our 90th percentile *M*-band result.

Theoretical planet models indicate that observations at the L' and *M* bands and the narrowband *H*-regime filter of Marois et al. (2006) can detect planets down to $3M_J$ in the Vega system. Further work at all three bands would either detect such a planet or rule out the existence of one at large separation with very high confidence. Consistent results at a variety of wavelengths will ensure that conclusions are less vulnerable to model uncertainties at any particular wavelength. More submillimeter work and orbital modeling of the Vega system is also desirable, because if models explaining the dust distribution without a massive planet can be ruled out, deep targeted AO observations to detect the planet could be strongly prioritized, and success could be anticipated with confidence.

5. ϵ ERI: COMPARISON WITH OTHER STUDIES AND UPPER LIMITS FOR HYPOTHETICAL PLANETS

5.1. *Comparing Our Sensitivity with Other Studies*

As with Vega, we do not attempt to compare our ϵ Eri results with an exhaustive list of other studies, but only with a few that obtained the best sensitivity results. We have chosen Itoh et al. (2006), Biller et al. (2007), and Lafrenière et al. (2007). Figure 15 shows the results of the comparison, again with the 90th percentile 10 σ sensitivity curves for our observations plotted.

Of the other studies, the sensitivity methods of Itoh et al. (2006) have already been discussed in § 4, as have those of Lafrenière et al. (2007), because we assumed that Marois et al. (2006) used the same methods for their Vega data. It only remains to consider the methods of Biller et al. (2007). They use a sensitivity estimator which is based on the single-pixel rms in 6 pixel (0.05″, or

1.2 λ/D) square boxes on the images, and they quote 5 σ limits. It is not clear whether they take processing losses into account in their sensitivity calculation. In general, we expect sensitivity estimators involving the single-pixel rms to overestimate the sensitivity, as they assume independence of noise in adjacent pixels. This assumption is always violated in the speckle-dominated regions on AO images (i.e., speckle noise is always spatially correlated, although the extent of the correlation depends on the details of the raw images and the type of PSF subtraction used).

The above would seem to imply that the Biller et al. (2007) 5 σ sensitivity results are comparable to our 5 σ limits, and that we should adjust them by a factor of 2 (0.753 mag) toward decreased sensitivity in order to compare them properly against our 10 σ limits. This would not include any correction for the possible overestimation of sensitivity in the presence of correlated noise.

However, several characteristics of the Biller et al. (2007) data suggest their sensitivity should be rated higher than this. First, they use a "roll subtraction" technique, which effectively creates both a positive and a negative image of any real companion, separated by 33° of rotation about the primary star, and the presence of both can be used to evaluate the reality of potential sources. This doubles the data, and the sensitivity should go up by $\sqrt{2}$ accordingly.

Second, their simultaneous differential imaging (SDI) technique involves two independent spectral differences. They are not necessarily equally sensitive, but in the best case this again doubles the data available for planet detection. With, potentially, four equal-brightness images of any real object in their data (two independent spectral difference images at each of two "roll angles"), the sensitivity of the Biller et al. (2007) observations should, in principle, go up by a factor of as much as 2 (i.e., $\sqrt{4}$) over their nominal values.

Finally, B. Biller has explained to us that the Biller et al. (2007) 5 σ point-source sensitivities were calculated by comparing the single-pixel rms noise to the brightness of the peak pixel of a PSF. This method is conservative for well-sampled data such as that of Biller et al. (2007), since it does not take into account the fact that bright pixels surrounding the peak of a PSF allow it to be detected with additional confidence. The single-pixel method also does not overestimate the sensitivity in the presence of correlated noise (provided the rms noise is calculated over a large enough region).

The above might indicate that we should compare the Biller et al. (2007) nominal 5 σ sensitivities directly to our 10 σ sensitivities (since obtaining four separate images of any real source could, in principle, raise the sensitivity to twice its nominal value). However, since the two spectral difference images do not necessarily have equal sensitivity, we have scaled the Biller et al. (2007) nominal 5 σ limits down in sensitivity by about a factor of $\sqrt{2}$ (0.38 mag) to compare them with our 10 σ limits. This is equivalent to taking into account the Biller et al. (2007) sensitivity gain only from the fact that an image is obtained in each of two roll angles, and not from the additional fact that at each roll angle two independent spectral difference images are produced. The reader should keep this in mind when examining Figure 15: we may have underestimated the relative sensitivity of the Biller et al. (2007) observations by a factor of around $\sqrt{2}$ (0.38 mag). This rather small correction would not affect our conclusions.

As with the Marois et al. (2006) Vega data (and also the Lafrenière et al. [2007] ϵ Eri data), we have adjusted the Biller et al. (2007) sensitivities toward greater sensitivity to convert magnitudes from narrowband filters tuned to a predicted peak in giant planet spectra to broadband H magnitudes. For Biller et al. (2007), the correction factor we applied was 0.84 mag. This is an approximate value based on the SDI observers' analysis of their own filters.

Figure 15 makes it clear that although the best H-regime results for Vega delivered better sensitivity than our L'- and M-band observations, the sensitivity of our M-band observation of ϵ Eri is better than that of all previous observations out to a separation of at least 7″ from the star. Within 3″ of the star the sensitivity advantage of the longer wavelength observation is especially great. We note that this applies only to our M-band result; the SDI method of Biller et al. (2007), which is designed to give excellent sensitivity close to bright stars, does give results comparable to those of our L' observation. The good performance of the M band is due to the fact that the planet/star flux ratio is much more favorable at the M band than even in the most optimized intervals of the H band.

In closing this section on comparative sensitivities, we note that although we have mainly used the theoretical planet models of Burrows et al. (2003) to calculate sensitivities in this work, those presented in Baraffe et al. (2003) are a good complement and comparison to the former. However, the filter set over which Baraffe et al. (2003) integrated their theoretical spectra is slightly different from the Clio filter set over which we integrated the Burrows et al. (2003) models. We have, however, also done tests in which we performed magnitude-mass conversions using the original mass/magnitude/age tables presented in Baraffe et al. (2003). In general, the Baraffe et al. (2003) models give us somewhat better sensitivity in L' than those of Burrows et al. (2003), with a typical disagreement of $1M_J$–$2M_J$. The M-band predictions of the two model sets are very close. At present we cannot say for sure if the L'-band discrepancy is inherent in the different models or is a pure artifact of the filter set. In any case the two model sets are broadly in agreement, except for very old, cool planets, where the differences become very large and it appears clear that slightly different filter sets cannot be the whole explanation (see the discussion of the H-band flux of ϵ Eri b below).

5.2. *Upper Limits at the Locations of Hypothetical Planets*

We note that ϵ Eri has the extremely important distinction of being one of only a few stars around which a single planet has been detected with both RV and astrometric methods (Hatzes et al. 2000; Benedict et al. 2006). This means that a complete, unique solution for the size, eccentricity, and orientation of the orbit is possible, as is a solution for the mass of the planet. Benedict et al. (2006) present such an orbit solution and give the mass of the planet as $1.55M_J$.

At the time of our observations the Benedict et al. (2006) orbit predicts a separation of about 0.684″. Our observations do not set upper limits on the planetary mass regime this close to the star. We note, however, that our observations were not timed with the idea of obtaining good sensitivity to this planet. If we had observed the planet near its apastron, at which point the separation is about 1.7″, our M-band observations in particular would have been in the range to set possibly interesting limits, although still above the Benedict et al. (2006) mass of $1.55M_J$. The median 10 σ and 7 σ sensitivities of our M-band observation at 1.7″ are $5.3M_J$ and $4.2M_J$, respectively, and our 5 σ limit is $3.9M_J$. These are good sensitivities at a very small separation from a bright star, but, of course, the planet will still not be detected unless it is far more massive than the Benedict et al. (2006) orbital solution indicates. Could any current-technology telescope detect this planet, and if so, what would be the best method?

Janson et al. (2007) applied the same SDI methodology used by Biller et al. (2007) to observe ϵ Eri at several different epochs. The data from their second epoch gave them the best limit on the

planet, with a 3 σ sensitivity of Δ-magnitude 13.1 at the expected location of the planet based on Benedict et al. (2006). As discussed above, the Biller et al. (2007) observations using the SDI method had two independent roll angles and two independent spectral differences for each observation, and the sensitivity estimation method they used was conservative. Assuming that Janson et al. (2007) used the same methodology, we compare their 3 σ limits directly to our 10 σ limits. Note that, even considering all the issues mentioned in § 5.1, this results in a conservative estimation of our sensitivities relative to those of Janson et al. (2007).

We can adjust the Janson et al. (2007) 3 σ sensitivity of Δ-magnitude 13.1 by the 0.84 mag value used before and add the $H = 1.88$ mag of the star itself to get an equivalent sensitivity of $H = 15.8$; the equivalent masses are $9.6M_J$ and $9.1M_J$, according to the Burrows et al. (2003) and Baraffe et al. (2003) models, respectively, with the age set to 0.56 Gyr in both cases.

However, Janson et al. (2007) mention that the correction from the narrowband SDI filters to the H band would actually be much greater than 0.84 mag for a very cool object such as ϵ Eri b. According to their Figure 5, the correction is about 2.2 mag for the appropriate filter difference at our adopted age of 0.56 Gyr for ϵ Eri. This different correction does not change the upper limit of $9.6M_J$ quoted above, because the larger correction applies only to a planet with the $1.55M_J$ mass determined by Benedict et al. (2006), which would have been far too faint for Janson et al. (2007) to detect. However, the 2.2 mag correction is appropriate for estimating by what factor the Janson et al. (2007) observations missed the planet; that is, how much their sensitivity would have to be increased in order to detect it.

The sensitivity of the Janson et al. (2007) observations in their narrowband filter was about $13.1 + 1.88 = 14.98$ mag, assuming that the magnitude of ϵ Eri A is the same in the narrowband filter as in broadband H. According to the models of Burrows et al. (2003), a 0.56 Gyr old planet of mass $1.55M_J$ located 3.27 pc away has an H-band magnitude of about 28.5. We subtract the 2.2 mag correction to obtain a narrowband magnitude of 26.3 and difference the result with the Janson et al. (2007) sensitivity of 14.98 mag. The conclusion is that the Janson et al. (2007) sensitivity is insufficient to detect the planet by 11.3 mag (a factor of 34,000) under the Burrows et al. (2003) models. As noted in § 5.1, the Baraffe et al. (2003) models disagree with the Burrows et al. (2003) ones on the brightness of ϵ Eri b; the former indicate that the Janson et al. (2007) miss factor is only about 1000, rather than 34,000. The reason for this discrepancy is not clear. It does not affect our conclusions about the best band at which to search for ϵ Eri b. The large discrepancy for two model sets that are in close agreement for warmer objects does suggest that theoretical H-band magnitudes for objects with temperatures as low as ϵ Eri b have a large uncertainty, and therefore any constraints based on them will be tentative. The M-band brightnesses predicted by the two model sets for ϵ Eri b are discrepant by a much smaller factor, about 1.7 rather than 34 (see below).

The miss factors calculated above indicate that the SDI sensitivity would have to be increased at least a thousandfold to detect the planet. Assuming we had observed the planet at apastron, by what factor would we have failed to detect it? We consider only our M-band results, as they are more sensitive than our L' observations to low-mass planets close to the star. Our median 10 σ sensitivity at the apastron separation of 1.7″ was $M = 12.02$. The models of Burrows et al. (2003) give the brightness of the planet as $M = 14.7$. This means we would have come short of a 10 σ detection by 2.68 mag, or a factor of 11.8, according to the Burrows et al. (2003) models (the Baraffe et al. [2003] models give a higher but not enormously discrepant miss factor of 20.5; as we have up to this point, we focus on the Burrows et al. [2003] models in the discussion that follows). Our blind sensitivity tests indicate about 40% completeness at 5 σ, with 85% of sources at least noticed. Thus, if we could increase our sensitivity by only a factor of 5.9 (that is, 11.8 divided by 2 to change from 10 σ to 5 σ), we would have some chance of confidently detecting the planet, with a greater likelihood of at least noticing it.

These lower miss factors suggest that ϵ Eri b might actually be detectable near apastron with ground-based M-band imaging. It is almost certain that ϵ Eri b is at too low a $T_{\rm eff}$ for its M-band flux to be dimmed by the above-LTE CO concentrations suggested by Leggett et al. (2007) and Reid & Cruz (2002) to account for the suppressed M-band flux observed for much hotter objects (see Hubeny & Burrows [2007] for an analysis of how the effects of nonequilibrium CO concentrations diminish with decreasing $T_{\rm eff}$). We note also that even if the suppression of M-band flux remained, M would still be better for the detection than the H regime.

The next apastron of ϵ Eri b is in 2010, and this would be the best time to attempt to image it with a very deep M-band observation. We have observed that our sensitivity in both speckle-limited and background-limited regimes increases roughly as the square root of the integration time, as we would expect. Therefore, barring further improvements in Clio or MMTAO, an exposure 35 (or 5.9^2) times as long as our M-band integration would be required to have a 40% chance of making a confirmed detection of the planet using Clio at the MMT. This means 35 hr of observing, or about seven good nights. Improvements to the Clio instrument, MMTAO, and our processing methods might bring the detection in range with a shorter exposure, perhaps only two nights. We note that at 1.7″ from ϵ Eri our current images are speckle-limited; the background limit is still a factor of about 3 lower. Alterations to the instrument or improved PSF subtraction methods in postprocessing may, in future, obtain near-background-limited performance at this separation. The planet might then be detectable with only one or two nights' worth of integration, although four to six nights would still be preferred to ensure that an interesting upper limit could be set in the event of a nondetection. Clio has already been used with a phase plate coronagraph (Kenworthy et al. 2007), which improves the close-in sensitivity.

As far as we know, Clio, when used with the adaptive secondary AO system of the MMT, is the only currently operating AO imager able to make the deep, high-efficiency integrations in the broad M band required to detect ϵ Eri b. Other AO imagers exist that can use the M' band, where the narrower bandpass reduces the intensity of the thermal background. However, at M' the sensitivity to planets is also reduced, and the project becomes unfeasible. Given a multinight M-band integration with Clio, the goal of obtaining the first direct image of a mature extrasolar planet appears to be within reach.

Detection and characterization of ϵ Eri b should be quite straightforward with new large telescopes such as the Large Binocular Telescope (LBT; which might be used instead of the MMT to make the first detection), Giant Magellan Telescope (GMT), Thirty Meter Telescope (TMT), or European Extremely Large Telescope (E-ELT), provided the latter two are equipped with the adaptive secondary AO systems necessary to reduce thermal background and make deep M-band observations feasible. Space-based observations are likely to be useful as well. The planet might be studied at L', M-band, or longer wavelengths using the *James*

Webb Space Telescope (*JWST*), or it could be detected in reflected light at visible wavelengths by a sensitive space-based coronagraph. However, the first detection may come well ahead of *JWST* and the next generation of giant telescopes; it may be achieved in the *M* band with the MMT during the the 2010 apastron.

Ozernoy et al. (2000) and Quillen & Thorndike (2002) suggest that the dust disk of ϵ Eri has been sculpted by a planet of $0.1M_J$–$0.2M_J$ in an orbit between 40 and 65 AU in radius. Deller & Maddison (2005) agree and prefer the model of Quillen & Thorndike (2002). Such a planet would be far too faint to detect with any telescope in the near future. However, Deller & Maddison (2005) state that an additional, $\sim 1M_J$ planet in a closer-in orbit is likely required to produce the observed clearing of the dust inside about 30 AU (Greaves et al. 1998). The RV/astrometric planet of Hatzes et al. (2000) and Benedict et al. (2006) has too small an orbit to account for this dust clearing; Deller & Maddison (2005) suggest a larger orbital radius between 10 and 18 AU for the planet responsible for clearing the dust. Benedict et al. (2006) mention a long-term trend in RV measurements for ϵ Eri A that might indicate just such a planet: an $\sim 1M_J$ object orbiting with a period longer than 50 yr. Since such a planet would probably appear at least 3″–4″ from the star, we would likely have detected it if it had a mass of $4M_J$–$5M_J$ or greater, as would the Lafrenière et al. (2007) observation. Since the mass is expected to be closer to $1M_J$, it is not surprising that the planet has not yet been detected. It might be imaged serendipitously in the course of a very long exposure intended to detect the known RV/astrometric planet.

6. CONCLUSIONS

We have taken very deep L'- and *M*-band images of the interesting debris disk stars Vega and ϵ Eri to search each system for orbiting planets and brown dwarfs. For both stars we obtain better sensitivity than shorter wavelength observations at small separations from the star. The sensitivity of our observations compares more favorably to the sensitivity of *H*-regime observations in the case of ϵ Eri than in the case of Vega. For ϵ Eri, our *M*-band observation appears to set the best upper limits yet for planets out to a separation of about 7″, beyond which the sensitivity of the Lafrenière et al. (2007) *H*-regime observations becomes very slightly superior.

The reason our ϵ Eri observations have a greater sensitivity advantage over *H*-regime observations than do our images of Vega is the smaller distance to the ϵ Eri system. This is another instance of the same physical reality we discussed in § 3.3, when explaining why our *M*-band sensitivity is much better than our L' results on ϵ Eri but not on Vega. As we stated above, for ϵ Eri, the sensitivity of a given observation at any wavelength extends down to less luminous, lower $T_{\rm eff}$ planets than for Vega. The $H - L'$ and $H - M$ colors, as well as the $L' - M$ color, of low-$T_{\rm eff}$ giant planets are more red than those of hotter ones. Therefore, the faintest detectable objects in the ϵ Eri system would be more red than those in the more distant Vega system, and longer wavelength observations are most useful for the nearer system. This is a general and important principle for planning optimal planet-search strategies; the faintest detectable planets will be more red, and therefore the relative advantage of long wavelengths over short ones will be higher for the nearest stars. For distant stars where only hot objects with blue IR colors can be detected, long-wavelength observations are not as useful. For very nearby stars such as ϵ Eri, where very interesting, extremely low-mass, low-$T_{\rm eff}$ planets can be detected, the long wavelengths are very useful because the planets being sought have such red colors.

Planet-search observations at the L' and *M* bands have a considerable advantage over those in the more commonly used *H*-band regime for ϵ Eri and a handful of other bright, very nearby stars. For more distant bright stars such as Vega, L'- and *M*-band observations give markedly better results only at separations inside about 3″, and in this regime no currently employed method gives sensitivity to any but the highest mass planets. Observations in the bands we have employed are still useful on Vega, but their use tends toward a diversification of planet-search efforts in case theoretical models are overpredicting planets' *H*-band brightnesses. For nearer systems such as ϵ Eri, by contrast, L'- and *M*-band observations clearly provide the best sensitivity at the most interesting separations, and it is the *H*-regime images that naturally take the role of diversifying effort under the supposition that the models may overpredict planet brightness at longer wavelengths.

We have set a limit on the Vega planet hypothesized by Wilner (2004) that is close to the $3M_J$ mass he suggested for it. It appears that Marois et al. (2006) could set a similar limit. The evidence seems fairly strong that no $3M_J$ planet exists at this location. This favors alternative models involving smaller planets, such as those of Marsh et al. (2006) and Wyatt (2003), or a $3M_J$ planet in a larger orbit, such as that of Deller & Maddison (2005). Since a $3M_J$ planet around Vega could be imaged in multiple wavelength regimes with current technology, more submillimeter observations and further modeling to determine whether such a planet is required to explain the observed dust distribution is very desirable. If this does turn out to be the case, deep AO observations to detect the planet could be strongly prioritized, and a successful detection in one or more wavelength bands would be very likely.

Our ϵ Eri observation was not timed to catch the known planet ϵ Eri b at a large separation, and therefore our current data do not allow us to set an interesting limit on its mass. Janson et al. (2007) observed ϵ Eri at several epochs of more promising separation using SDI and set limits in the $9M_J$–$10M_J$ range.

We have set a limit of $4M_J$–$5M_J$ for additional planets in more distant orbits around ϵ Eri. The existence of a planet in such an orbit may be indicated by a long-term RV trend (Benedict et al. 2006) and by a clearing of dust from the inner disk (Deller & Maddison 2005). Benedict et al. (2006) and Deller & Maddison (2005) suggest a mass of around $1M_J$ for this hypothetical outer planet, so our nondetection is not surprising.

We have explored the question of whether SDI imaging (Janson et al. 2007; Biller et al. 2007) or L'- and *M*-band imaging (this work) is the method most likely to ultimately detect ϵ Eri b. Our *M*-band images were much more sensitive at small separations than our L' results, so we have not considered the latter. We find that the sensitivity of the Janson et al. (2007) observations at the best epoch, where the planet is near the optimal separation for SDI imaging, is still insufficiently sensitive to detect the planet by a factor of at least 1000. By contrast, our observations, if carried out at apastron, would have missed the planet by a factor of only about 12.

This striking difference suggests that it is at the *M* band that the planet ϵ Eri b will first be imaged. A several-night observing campaign using Clio at the MMT might detect it during the 2010 apastron passage, since we have observed that the sensitivity in the speckle-dominated regions of *M*-band images does go up approximately as the square root of the exposure time. More advanced PSF subtraction or coronagraphic capability in Clio (Kenworthy et al. 2007) might reduce the required exposure time to detect the planet to as little as two nights. At present, we believe Clio with MMTAO is the only system capable of deep planet-imaging integrations in the *M* band. *Spitzer*, despite its

enormously lower background and correspondingly excellent sensitivity, does not have sufficient resolution to detect objects at the separations expected for orbiting planets.

New giant telescopes such as the LBT and GMT with planned adaptive secondary AO systems could be used to study ϵ Eri b in more detail. The *M* band will remain the best wavelength choice for observations using these larger telescopes, so adaptive secondaries will remain essential; conventional AO systems, even on giant telescopes, will likely still have too high a thermal background for efficient, deep *M*-band images. An L'- and *M*-band imager called LMIRCam is planned for the LBT (Wilson et al. 2007). When *JWST* is launched, it should also deliver interesting scientific results on ϵ Eri b. However, it is possible that the first image of this planet—the first direct image of any mature extrasolar planet—will be obtained using Clio at the MMT in 2010.

This research has made use of the SIMBAD database, operated at CDS, Strasbourg, France. This research has made extensive use of information and code from Press et al. (1992). We thank I. Baraffe for kindly supplying us with theoretical spectrum files corresponding to the planet models used in Baraffe et al. (2003). We thank the referee, Remi Soummer, for helpful comments.

Facilities: MMT

REFERENCES

Aumann, H. 1985, PASP, 97, 885
Aumann, H., et al. 1984, ApJ, 278, L23
Backman, D. 1996, BAAS, 28, 1056
Baraffe, I., Chabrier, G., Barman, T. S., Allard, F., & Hauschildt, P. H. 2003, A&A, 402, 701
Benedict, G., et al. 2006, AJ, 132, 2206
Biller, B. A., et al. 2006, Proc. SPIE, 6272, 62722D
———. 2007, ApJS, 173, 143
Burrows, A., Sudarsky, D., & Lunine, J. I. 2003, ApJ, 596, 587
Deller, A., & Maddison, S. 2005, ApJ, 625, 398
Fischer, D. 1998, Ph.D. thesis, Univ. California, Santa Cruz
Freed, M., Hinz, P., Meyer, M., Milton, N., & Lloyd-Hart, M. 2004, Proc. SPIE, 5492, 1561
Geissler, K. et al. 2007, A&A, 461, 665
Greaves, J., et al. 1998, ApJ, 506, L133
Hatzes, A., et al. 2000, ApJ, 544, L145
Hinkley, S., et al. 2007, ApJ, 654, 633
Hinz, P., Heinze, A., Sivanandam, S., Miller, D., Kenworthy, M., Brusa, G., Freed, M., & Angel, J. 2006, ApJ, 653, 1486
Hubeny, I., & Burrows, A. 2007, ApJ, 669, 1248
Itoh, Y., Oasa, Y., & Fukagawa, M. 2006, ApJ, 652, 1729
Janson, M., et al. 2007, AJ, 133, 2442
Kenworthy, M., Codona, J., Johanan, L., Hinz, P., Angel, J., Heinze, A., & Sivanandam, S. 2007, ApJ, 660, 762
Lafrenière, D., et al. 2007, ApJ, 670, 1367
Leggett, S., Saumon, D., Marley, M., Geballe, T., Golimowksi, D., Stephens, D., & Fan, X. 2007, ApJ, 655, 1079
Leggett, S., et al. 2003, MNRAS, 345, 144
Li, A., & Lunine, J. 2003, ApJ, 590, 368
Marley, M. S., Fortney, J. J., Hubickyj, O., Bodenheimer, P., & Lissauer, J. J. 2007, ApJ, 655, 541
Marois, C., Lafrenière, D., Doyon, R., Macintosh, B., & Nadeau, D. 2006, ApJ, 641, 556
Marsh, K., Dowell, C., Velusamy, T., Grogan, K., & Beichman, C. 2006, ApJ, 646, L77
Masciadri, E., Mundt, R., Henning, Th., Alvarez, C., & Barrado y Navascués, D. 2005, ApJ, 625, 1004
Neuhäuser, R., Brandner, W., Eckart, A., Guenther, E., Alves, J., Ott, T., Huélamo, N., & Fernández, M. 2000, A&A, 354, L9
Ozernoy, L., Gorkavyi, N., Mather, J., & Taidakova, T. 2000, ApJ, 537, L147
Press, W. H., Teukolsky, S. A., Vetterling, W. T., & Flannery, B. P. 1992, Numerical Recipes in C (2nd ed.; New York: Cambridge Univ. Press)
Quillen, A., & Thorndike, S. 2002, ApJ, 578, L149
Reid, I., & Cruz, K. 2002, AJ, 123, 466
Sivanandam, S., Hinz, P., Heinze, A., & Freed, M. 2006, Proc. SPIE, 6269, 27
Song, I., Caillault, J.-P., Barrado y Navascués, D., & Stauffer, J. 2001, ApJ, 546, 352
Vikhlinin, A., Forman, W., Jones, C., & Murray, S. 1995, ApJ, 451, 542
Wilner, D. 2004, in ASP Conf. Ser. 324, Debris Disks and the Formation of Planets, ed. L. Caroff et al. (San Francisco: ASP), 241
Wilson, J., Hinz, P., Kenworthy, M., Skrutskie, M., Jones, T., Nelson, M., Woodward, C., & Garnavich, P. 2007, in Proc. Conf. in the Spirit of Bernard Lyot: The Direct Detection of Planets and Circumstellar Disks in the 21st Century, ed. P. Kalas (Berkeley: Univ. California), 51
Wyatt, M. 2003, ApJ, 598, 1321